arXiv:1402.5141v1 [cond-mat.stat-mech] 20 Feb 2014

Long-time behavior of periodically driven isolated interacting quantum systems

Luca D'Alessio[1,2] and Marcos Rigol[1]

[1] *Department of Physics, The Pennsylvania State University, University Park, PA 16802, USA*
[2] *Department of Physics, Boston University, Boston, MA 02215, USA*

We show that finite isolated and interacting quantum systems under a periodic drive exhibit three physical regimes. For short driving periods the Floquet Hamiltonian is well approximated by the time-averaged Hamiltonian, while for long periods the evolution operator exhibits properties of random matrices of a Circular Ensemble (CE). In-between, there is a crossover regime. We argue that, in the thermodynamic limit and for nonvanishing driving periods, the evolution operator always exhibits properties of CE random matrices. Consequently, driving leads to infinite temperature at infinite time and to an unphysical Floquet Hamiltonian.

Introduction. Periodically driven systems have a long history, one paradigmatic example is the Kicked-Rotor model of a particle moving on a ring subjected to time-periodic "kicks" [1]. The behavior of such systems is very rich, e.g., they can display interesting integrability-to-chaos transitions and dynamical Anderson localization [2, 3] and counter intuitive effects such as dynamical stabilization [4, 5] both in classical and quantum mechanics. Moreover, it has been recently shown that periodic perturbation can be used as a flexible experimental knob [6–8] to realize synthetic matter, i.e., matter with specific engineered properties. Two outstanding examples in this direction are the opening of a gap in graphene by using light or carefully selected lattice phonons [9–11] and the realization of the so called Floquet topological insulator in a material which, in absence of the driving, is topologically trivial [12, 13].

With a few exceptions [14–18], recent studies mostly focus on driving simple (often single-particle) Hamiltonians. Furthermore, theoretical analyses often rely on approximations that allow one to recast the effect of the drive in, e.g., an effective hopping [19, 20]. The validity of some of those approximations, such as the use of average Hamiltonians, has been a topic of interest for many years because of its relevance to NMR experiments [21, 22]. Our goal in this Letter is to understand the long-time behavior of generic isolated quantum systems under a periodic drive. We pay special attention to the role of finite size effects, which may be relevant to experiments with ultracold gases. Combining theoretical arguments and numerical results we argue that finite systems exhibit three different regimes, while only one survives in the thermodynamic limit. In the latter, the system approaches infinite temperature at infinite time and the Floquet Hamiltonian becomes unphysical, i.e. it cannot be an extensive operator with few-body interactions.

Theoretical Analysis. The Floquet theorem states that the dynamics of periodically driven systems can be described by the time-independent Floquet Hamiltonian, $\hat{H}_F$, defined by:

$$\hat{U}_{\rm cycle} \equiv \exp\left[T\,\frac{\hat{H}_F}{i\hbar}\right] = \sum_n |\phi_n\rangle e^{-i\theta_n}\langle\phi_n|, \qquad (1)$$

where T is the period of the driving, $\hat{U}_{\rm cycle}$ is the exact evolution operator over a full cycle and $|\phi_n\rangle$ and $e^{-i\theta_n}$ are its eigenstates and eigenvalues. From Eq. (1) if follows that $H_F \equiv \sum_n |\phi_n\rangle\varepsilon_n\langle\phi_n|$ where the Floquet energies, ε_n, can be shifted by integers of $2\pi\hbar/T$ without violating (1). We stress that $\hat{H}_F$ does not need to be a physical Hamiltonian. For example, $\hat{H}_F$ may contain many-body interactions and may not be extensive. Moreover, in general, it is not possible to evaluate $\hat{H}_F$ explicitly and one has to rely on approximations such as the Magnus expansion [23]. The latter is a perturbative expansion in T, which is guaranteed to converge for finite-dimensional Hamiltonians and sufficiently short periods [24].

Here we follow a different approach [21]. We introduce a generic time-periodic local Hamiltonian $\hat{H}(\tau)$

$$\hat{H}(\tau) = \hat{H}_{\rm ave} + f(\tau)\hat{A}, \quad \hat{H}(\tau)|n(\tau)\rangle = \epsilon_n(\tau)|n(\tau)\rangle, \quad (2)$$

where $\tau \equiv t/T$ is the rescaled time, T is the driving period, $f(\tau)$ is an arbitrary time-periodic function $[f(\tau+1) = f(\tau)]$ with zero average $[\int_0^1 d\tau\, f(\tau) = 0]$, $\hat{H}_{\rm ave}$ is the time-averaged Hamiltonian, and $\hat{A}$ is a sum of local few-body operators. $|n(\tau)\rangle$ and $\epsilon_n(\tau)$ are the instantaneous eigenfunctions and eigenenergies of $\hat{H}(\tau)$. The Schrödinger equation reads

$$\partial_\tau \hat{U}(\tau) = T\,\frac{\hat{H}(\tau)}{i\hbar}\hat{U}(\tau), \qquad (3)$$

which is formally solved by

$$\hat{U}(\tau) = \mathcal{T}\exp\left[T\int_0^\tau d\tau'\frac{\hat{H}(\tau')}{i\hbar}\right] \equiv \exp\left[T\,\frac{\hat{H}_{\rm eff}(\tau)}{i\hbar}\right], \qquad (4)$$

where $\mathcal{T}$ ensures that the exponential is time-ordered. The last equality is the definition of the effective Hamiltonian $\hat{H}_{\rm eff}(\tau)$. From Eqs. (1) and (4) one can see that $\hat{H}_{\rm eff}(\tau=1) \equiv \hat{H}_F$. In what follows, $|\phi_n(\tau)\rangle$ and $\varepsilon_n(\tau)$ indicate the instantaneous eigenstates and eigenenergies of $\hat{H}_{\rm eff}(\tau)$ $[\hat{H}_{\rm eff}(\tau)|\phi_n(\tau)\rangle = \varepsilon_n(\tau)|\phi_n(\tau)\rangle]$, and, as before, $|\phi_n\rangle \equiv |\phi_n(\tau=1)\rangle$ and $\varepsilon_n \equiv \varepsilon_n(\tau=1)$ denote the eigenstates and eigenenergies of $\hat{H}_F$. Equations (3) and

(4) lead to the fundamental relation [21, 25]

$$\frac{i\hbar}{T}\frac{e^{\frac{T}{i\hbar}\Delta\varepsilon_{n,m}(\tau)}-1}{\Delta\varepsilon_{n,m}(\tau)}\langle\phi_n(\tau)|\partial_\tau\hat{H}_{\rm eff}(\tau)|\phi_m(\tau)\rangle = \langle\phi_n(\tau)|\hat{H}(\tau)|\phi_m(\tau)\rangle, \tag{5}$$

where we have defined $\Delta\varepsilon_{n,m}(\tau)\equiv\varepsilon_n(\tau)-\varepsilon_m(\tau)$. From Eq. (5), using the identity $\lim_{x\to 0}\frac{e^x-1}{x}=1$ and the Hellmann-Feynman theorem, for $m=n$ we obtain [25]

$$\partial_\tau\varepsilon_n(\tau)=\langle\phi_n(\tau)|\hat{H}(\tau)|\phi_n(\tau)\rangle, \tag{6}$$

and for $n\neq m$

$$\frac{i\hbar}{T}\left(1-e^{\frac{T}{i\hbar}\Delta\varepsilon_{n,m}(\tau)}\right)\langle\phi_n(\tau)|\partial_\tau|\phi_m(\tau)\rangle = \langle\phi_n(\tau)|\hat{H}(\tau)|\phi_m(\tau)\rangle. \tag{7}$$

Equations (5)–(7) are central to our analysis. They are exact and can be integrated numerically to obtain $\hat{H}_{\rm eff}(\tau=1)\equiv\hat{H}_F$. They can also be used to determine $\hat{H}_F$ perturbatively.

In the limit $T\,\Delta\varepsilon_{n,m}(\tau)/\hbar\ll 1$, one can expand the exponential in Eq. (5), and, to first order, the dependence on the period T disappears

$$\langle\phi_n(\tau)|\partial_\tau\hat{H}_{\rm eff}(\tau)|\phi_m(\tau)\rangle=\langle\phi_n(\tau)|\hat{H}(\tau)|\phi_m(\tau)\rangle \Rightarrow \partial_\tau\hat{H}_{\rm eff}(\tau)=\hat{H}(\tau)$$

where we have used the fact that $|\phi_n(\tau)\rangle$ is an orthonormal basis. The equation above is equivalent to $\hat{H}_F=\int_0^1 d\tau\,\hat{H}(\tau)=\hat{H}_{\rm ave}$. In this limit, ε_n are extensive, i.e. proportional to the volume of the system, V. Therefore, $\Delta\varepsilon_{n,m}(\tau)$ between the lowest and highest eigenstates of $\hat{H}_F$ is $\propto V$ and, in order for the expansion of the exponential $\forall\, n,m,\tau$ to be meaningful, one needs $T\ll{\rm const}/V$. In this limit, the phases of the evolution operator are proportional to the eigenenergies of $\hat{H}_{\rm ave}$. We note that the condition $T\ll{\rm const}/V$ is only a sufficient condition for $\hat{H}_F=\hat{H}_{\rm ave}$. For example, if $\hat{H}(\tau)$ commutes at different times, $[H(\tau),H(\tau')]=0$, then it trivially follows that $\hat{H}_F=\hat{H}_{\rm ave}$ independently of T.

Remarkably, evaluating Eq. (7) at $\tau=1$ allows one to connect the structure of the eigenstates of $\hat{H}_F$ to the statistics of the phases of the evolution operator. When the eigenstates $\hat{H}_F$ are chaotic, the RHS of (7) would be generically non-zero for any pair of states (this follows from recalling that $\hat{H}(\tau=1)$ is a sum of local few-body operators) and the phases of $\hat{U}_{\rm cycle}$ are expected to display repulsion [see LHS of Eq. (7)]. On the other hand, if $\hat{H}_F$ is noninteracting (or integrable) then the RHS of Eq. (7) can be zero for a large fraction of pairs of states and there needs not be repulsion in the phases. In this case, the spectrum of $\hat{U}_{\rm cycle}$ could exhibit highly degenerate phases separate by finite gaps.

We should stress that, for $T>T_c=2\pi/W$, repulsion in the phases of $\hat{U}_{\rm cycle}$ is incompatible with $\hat{H}_F=\hat{H}_{\rm ave}$, where $W=\epsilon^{\rm ave}_{\rm max}-\epsilon^{\rm ave}_{\rm min}\propto V$ is the width of the spectrum of the average Hamiltonian. This because, for $\hat{H}_F=\hat{H}_{\rm ave}$, the phases would be $\theta_n=T\epsilon^{\rm ave}_n/\hbar$ and would not exhibit repulsion. The same reasoning leads to the conclusion that, for $T>T_c$, repulsion in the phases is incompatible with $\hat{H}_F$ being an extensive operator with few-body interactions. This type of operators do not have correlations between far-away energies levels and, therefore, can not produce repulsion for the phases. Actually, repulsion of the phases of $\hat{U}_{\rm cycle}$ for $T>T_c$ hints [see Eq. (7)] that $\hat{U}_{\rm cycle}$ should exhibit properties of random matrices belonging to the Circular Ensembles (CEs) [26–29]. CEs are the equivalent of Gaussian Ensembles (GEs) for unitary matrices. In CEs the phases display repulsion and the eigenstates are essentially random vectors [so that both sides of Eq. (7) are generically different from zero].

Numerical Results. We now turn to numerical simulations to understand what happens when one drives a realistic many-body system. Specifically, we use full exact diagonalization to study a spin-1/2 chain with periodic boundary conditions and Hamiltonian

$$\hat{H}(t)=\left[J+f(t)\,\delta J\right]\hat{H}_{nn}+J'\sum_j\sigma^z_j\sigma^z_{j+2}, \tag{8}$$

$$\hat{H}_{nn}=\sum_j\left[\sigma^z_j\sigma^z_{j+1}-\frac{1}{2}\left(\sigma^x_j\sigma^x_{j+1}+\sigma^y_j\sigma^y_{j+1}\right)\right],$$

where σ^α_j, $\alpha=x,y,z$, is the Pauli matrix for the $j^{\rm th}$ spin, $f(t)$ is a periodic function with zero average, $f(t)=1$ for $N<t/T<N+\frac{1}{2}$ and $f(t)=-1$ for $N+\frac{1}{2}<t/T<N+1$. The Hamiltonian (8) is relevant to nuclear magnetic resonance experiments in solids [30]. The next-nearest neighbor coupling J' can be considered to be a phenomenological parameter that accounts for interactions that break the integrability of the spin-1/2 XXZ chain. We restrict our calculations to the sector with total momentum $k=0$, magnetization $m_z=1/3$, and parity $p=+1$. For the largest system size considered ($L=24$ spins) that sector contains $D=15581$ states. The Hamiltonian parameters are $J=1$, $\delta J=0.2$, and $J'=0.8$. They have been chosen to ensure that the average Hamiltonian is non-integrable and exhibits eigenstate thermalization [25, 31–33]. Given the time dependence chosen, we obtain the exact evolution operator over one cycle $\hat{U}_{\rm cycle}=\exp[T\hat{H}_+/(2i\hbar)]\exp[T\hat{H}_-/(2i\hbar)]$, where $\hat{H}_\pm$ corresponds to Eq. (8) for $f(t)=\pm1$.

We are first interested in understanding the properties of the phases θ_n (obtained diagonalizing $\hat{U}_{\rm cycle}$) when compared to those obtained if $\hat{H}_F=\hat{H}_{\rm ave}$, i.e, $\theta^{\rm ave}_n=T\epsilon^{\rm ave}_n/\hbar$, as a function of the driving period T. In recent studies, the ratio of two consecutive energy gaps [34, 35] has been proven to be a good quantum chaos indicator. We extend this idea to our setup [25] and measure the statistics of $r=\frac{\min(\delta_n,\delta_{n+1})}{\max(\delta_n,\delta_{n+1})}$, where we have defined

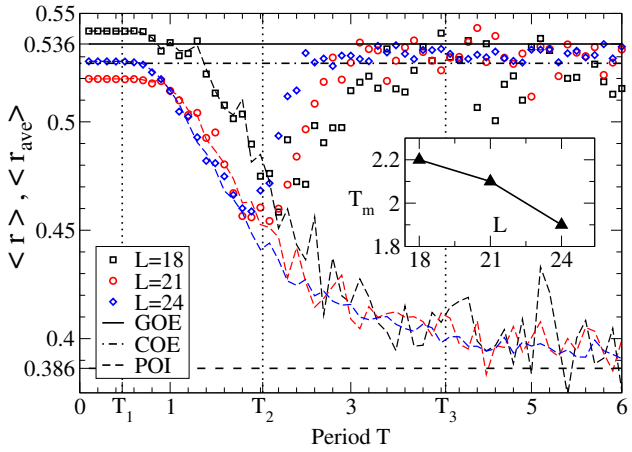

FIG. 1. (Color online) Average value of r vs the period T. The values of $\langle r\rangle$ (symbols) and $\langle r_{\rm ave}\rangle$ (dashed lines) are compared to the COE, GOE and POI predictions. The COE and GOE predictions are expected to coincide in the thermodynamic limit [25]. Vertical dotted lines depict the periods $T_1 = 2\pi\hbar/W$, $T_2 = \pi\hbar/\sigma$, and $T_3 = 2\pi\hbar/\sigma$, where W is the width of the full spectrum and σ is the width of the Gaussian that best fits the density of states for $L = 24$ (W and σ are $\propto L$ [25]). (Inset) The period T_m at which $\langle r\rangle$ is minimum decreases with increasing system size.

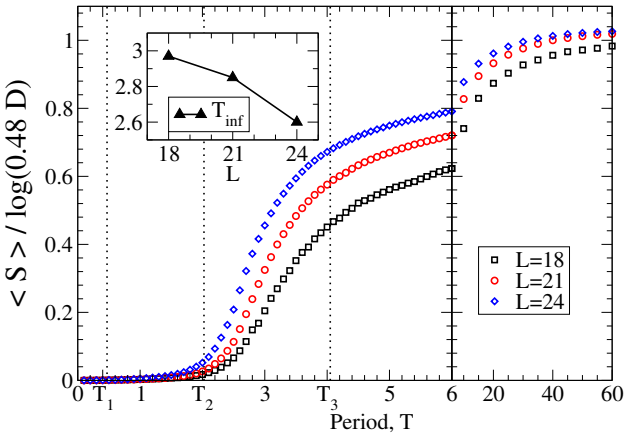

FIG. 2. (Color on-line) Average entropy of the eigenstates $\langle S\rangle$ vs the period T. $\langle S\rangle/\ln(0.48D)$ crosses-over from zero to the COE prediction, which is reached earlier as L increases. The variance $\langle(S_n - \langle S\rangle)^2\rangle^{1/2}$ is smaller than the size of the symbols used. (Inset) Period $T_{\rm inf}$ at which the diagonal entropy has an inflection point vs L.

the phase gap $\delta_n \equiv \theta_{n+1} - \theta_n$. Values of r close to zero indicate the lack of phase repulsion. In Fig. 1, we show the average value of r for different values of T for the exact phases θ_n (indicated by $\langle r\rangle$) and the phases $\theta_n^{\rm ave}$ (indicated by $\langle r_{\rm ave}\rangle$) and compare them with the predictions of the Circular Orthogonal Ensemble (COE), the Gaussian Orthogonal Ensemble (GOE), and Poisson statistics (POI). The COE and GOE predictions in Fig. 1 have been computed for matrix of finite size and are expected to coincide in the thermodynamic limit [25].

In Fig. 1, we observe four regions in which $\langle r\rangle$ and $\langle r_{\rm ave}\rangle$ exhibit distinctive behavior. Note the vertical dotted lines that mark T_1, T_2, and T_3 (see Fig. 1 caption). i) For $T < T_1$, $\langle r\rangle$ is independent of T, identical to $\langle r_{\rm ave}\rangle$, and close to the GOE prediction. ii) For $T_1 < T < T_2$, $\langle r\rangle$ and $\langle r_{\rm ave}\rangle$ are very close to each other and decrease with increasing T. iii) For $T_2 < T < T_3$, $\langle r\rangle$ increases towards the COE prediction while $\langle r_{\rm ave}\rangle$ decreases towards the POI prediction. iv) For $T > T_3$, $\langle r\rangle$ is again independent of T and close to the COE prediction, while $\langle r_{\rm ave}\rangle$ is very close and continues approaching the POI prediction. In the inset, we track the period T_m at which $\langle r\rangle$ has its minimum. t can be seen to decrease with increasing system size.

Further insights on our driven system can be gained by studying the properties of the eigenvectors of $\hat{U}_{\rm cycle}$. Specifically, we would like to understand how they become different from the eigenvectors of $\hat{H}_{\rm ave}$ as one increases T. We write the former in terms of the latter, $|\phi_n\rangle = \sum_{m=1}^{D} c_m^n |m_{\rm ave}\rangle$, where $\hat{H}_{\rm ave}|m_{\rm ave}\rangle = \epsilon_m^{\rm ave}|m_{\rm ave}\rangle$ and D is the dimension of the Hilbert space, and compute the (Shannon) information entropy [33]

$$S_n = -\sum_{m=1}^{D} |c_m^n|^2 \ln |c_m^n|^2, \qquad (9)$$

which measures the number of states $|m_{\rm ave}\rangle$ that contribute to each $|\phi_n\rangle$. When $\hat{H}_F = \hat{H}_{\rm ave}$, $S_n = 0$. As $\hat{H}_F$ deviates from $\hat{H}_{\rm ave}$, S_n grows and it is expected to saturate at the COE prediction $S_n \approx \ln(0.48D)$.

In Fig. 2, we show the average entropy $\langle S\rangle = \left(\sum_{n=1}^{D} S_n\right)/D$ normalized by the COE prediction. We note that $\langle S\rangle$ grows monotonically with increasing the period and that the curves shift to the left as the system size increases. The latter is also seen in the inset, where we plot the period $T_{\rm inf}$ at which each curve has an inflection point vs L. The variance $\langle(S_n - \langle S\rangle)^2\rangle^{1/2}$ is smaller than the size of the symbols used in Fig. 2. This makes apparent that, in average, eigenstates $|\phi_n\rangle$ delocalize the same way in the basis $\{|m_{\rm ave}\rangle\}$. Contrary to $\langle r\rangle$ (in Fig. 1), $\langle S\rangle$ (in Fig. 2) is still changing for $T \geq T_3$. However, the COE prediction is reached for longer periods. This is not surprising since indicators based on the eigenvectors are known to suffer from stronger finite-size effects than level statistics indicators [33].

The fact that $\hat{U}_{\rm cycle}$ shares properties of a COE has important consequences in the energy absorption of the system. To show it, we compute the expectation value of $\hat{H}_{\rm ave}$ at time $t = NT$ for $N \to \infty$. This can be done using the so-called diagonal ensemble [32]

$$\langle \hat{H}_{\rm ave}\rangle(t = NT) = \langle\psi_0| \left(\hat{U}_{\rm cycle}^{\dagger}\right)^N \hat{H}_{\rm ave} \left(\hat{U}_{\rm cycle}\right)^N |\psi_0\rangle$$
$$\approx \sum_n |\langle\psi_0|\phi_n\rangle|^2 \langle\phi_n|\hat{H}_{\rm ave}|\phi_n\rangle. \qquad (10)$$

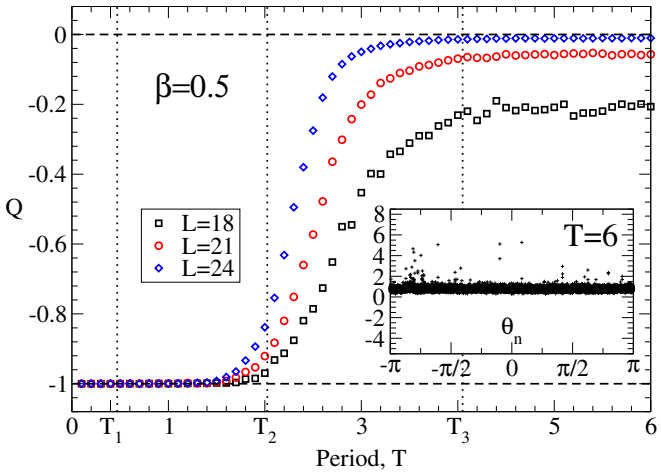

FIG. 3. (Color on-line) Absorbed energy. (Main) Absorbed energy at infinite time Q (see text) vs the driving period T. The initial state is a thermal state (with respect $\hat{H}_{\rm ave}$) with $\beta = 0.5$. (Inset) Expectation values $\langle\phi_n|\hat{H}_{\rm ave}|\phi_n\rangle$ vs the exact phases θ_n for $L = 24$ and $T = 6$.

In the COE all eigenstates are essentially random vectors and the expectation value of few-body observables become n-independent [25]. This occurs in our system for $\langle\phi_n|\hat{H}_{\rm ave}|\phi_n\rangle$ when $T > T_3$, as shown in the inset in Fig. 3 for $T = 6$ and $L = 24$. Hence, for $T > T_3$, the evaluation of Eq. (10) gives a result that corresponds to infinite temperature independently of $|\psi_0\rangle$.

In Fig. 3, we show the energy absorbed at infinite time Q vs T. We have normalized Q so that -1 corresponds to no-energy absorption and 0 corresponds to the final energy being equal to that at infinite temperature, i.e., $Q = \frac{\langle\hat{H}_{\rm ave}\rangle(t\to\infty)-\langle\hat{H}_{\rm ave}\rangle_{\beta=0}}{\langle\hat{H}_{\rm ave}\rangle_{\beta=0}-\langle\hat{H}_{\rm ave}\rangle(t=0)}$. The initial state is taken to be in thermal equilibrium (with respect to $\hat{H}_{\rm ave}$) with $\beta = 0.5$. Namely, $|\psi_0\rangle\langle\psi_0| = Z^{-1}\sum_m e^{-\beta E^{\rm ave}_m}|m_{\rm ave}\rangle\langle m_{\rm ave}|$, where Z is the partition function. Figure 3 shows that, with increasing T, Q approaches zero as expected. In addition, the value of T at which Q saturates close to zero decreases with increasing system size.

Discussion. Our numerical results support the initial conclusion that $\hat{H}_F = \hat{H}_{\rm ave}$ for vanishingly small values of T ($T \ll T_2$ in our case), while $\hat{U}_{\rm cycle}$ shares properties of matrices of the COE for larger values of T ($T \gg T_3$ in our case). In finite systems, there is a cross-over regime (for intermediate periods T) in which some indicators (repulsion between consecutive levels) have already reached the COE predictions while others (the information entropy of eigenstates) have not (see Figs. 1 and 2). In this regime, a drive may lead to states in which the average energy in a cycle fluctuates between consecutive cycles or becomes stationary but not equal to the infinite temperature expectation value. This could be seen in current experiments with periodically driven cold-atomic systems.

The scaling of our results with system size (see Figs. 1–3) suggests that, in the thermodynamic limit, any nonvanishing driving period T leads to an evolution operator $\hat{U}_{\rm cycle}$ that shares properties with random matrices of the COE. As a result, the system reaches the infinite temperature limit for infinite driving times. When this occurs, the Floquet Hamiltonian $\hat{H}_F$ cannot be an extensive Hamiltonian with few-body interactions because the latter would not produce phase repulsion for nonvanishing values of T. Therefore finite interacting systems driven at intermediate periods offer a natural platform to investigate unique phenomena that may occur as a result of long-range and/or many-body interactions in $\hat{H}_F$.

While we expect that our conclusions apply to generic interacting many-body systems, there are specific classes of models that could lead to $\hat{H}_F$ being a well-behaved local Hamiltonian over a finite range of driving periods. Examples are, (i) driven Hamiltonians that commute at different times, $\left[\hat{H}(\tau), \hat{H}(\tau')\right] = 0$, which lead to $\hat{H}_F = \hat{H}_{\rm ave}$ independently of T (in this case both the LHS and RHS of Eq. (7) are identically zero), ii) fictitious time-dependence that can be removed by a proper choice of the reference frame (see, e.g., [11]), iii) special situations in which multiple commutators of $\hat{H}(\tau)$ generate a finite algebra [14, 37].

In conclusion we have shown that isolated finite interacting systems subjected to a periodic driving exhibit three possible physical regimes. For short driving period T, $\hat{H}_F$ converges to the time-averaged Hamiltonian $\hat{H}_{\rm ave}$, while for large periods the evolution operator $\hat{U}_{\rm cycle}$ shares properties of matrices of the COE of random matrix theory. For intermediate periods, we find that there is a cross-over regime in which some indicators have already approached the COE predictions while others have not. In the latter regime finite systems may exhibit unexpected behavior, e.g., they may not heat up to infinite temperature and may reach interesting stationary states that could be observed in current experiments with cold-atomic systems. We have provided evidence that, in the thermodynamic limit, the only regime that occurs for nonvanishing driving periods is the one in which $\hat{U}_{\rm cycle}$ exhibits properties of COE random matrices. This results in the system heating up to infinite temperature at infinite times (see Fig. 3). Furthermore, $\hat{H}_F$ cannot be an extensive Hamiltonian with few-body interaction in that regime. An exciting question that we plan to explore next is the effect of a thermal bath on the dynamics of interacting periodically driven systems [22, 38–40].

Acknowledgments. We thank M. Bukov, I. Iadecola, A. Polkovnikov and L. F. Santos for many stimulating conversations. This work was supported by the office of Naval Research.

SUPPLEMENTARY INFORMATION.

DERIVATION OF EQS. (5)

Here, for completeness, we report the derivation of Eq. (5). Our presentation follows closely Ref. [21]. By plugging the ansatz (4) in the SE equation (3) one obtains

$$\partial_\tau \exp\left[T\,\frac{\hat{H}_{\rm eff}(\tau)}{i\hbar}\right] = T\,\frac{\hat{H}(\tau)}{i\hbar}\,\exp\left[T\,\frac{\hat{H}_{\rm eff}(\tau)}{i\hbar}\right].$$

Using the mathematical identity

$$\partial_\tau \exp\left[\hat{B}(\tau)\right] = \int_0^1 d\alpha\,\left(\exp\left[\alpha\,\hat{B}(\tau)\right]\,\partial_\tau\hat{B}(\tau)\,\exp\left[(1-\alpha)\,\hat{B}(\tau)\right]\right),$$

to compute the derivative of an exponential operator (note that this expression is required because $\hat{H}_{\rm eff}(\tau)$ at different times may not commute) results in

$$\int_0^1 d\alpha\,\left(\exp\left[\alpha\,T\,\frac{\hat{H}_{\rm eff}(\tau)}{i\hbar}\right]\,\partial_\tau\hat{H}_{\rm eff}(\tau)\,\exp\left[(1-\alpha)\,T\,\frac{\hat{H}_{\rm eff}(\tau)}{i\hbar}\right]\right) = \hat{H}(\tau)\,\exp\left[T\,\frac{\hat{H}_{\rm eff}(\tau)}{i\hbar}\right].$$

Multiplying both sides in the equation above by $\exp\left[-T\,\frac{\hat{H}_{\rm eff}(\tau)}{i\hbar}\right]$ from the right one gets

$$\int_0^1 d\alpha\,\left(\exp\left[\alpha\,T\,\frac{\hat{H}_{\rm eff}(\tau)}{i\hbar}\right]\,\partial_\tau\hat{H}_{\rm eff}(\tau)\,\exp\left[-\alpha\,T\,\frac{\hat{H}_{\rm eff}(\tau)}{i\hbar}\right]\right) = \hat{H}(\tau). \tag{11}$$

We now close this equation between the exact (time-dependent) eigenstates of $H_{\rm eff}(\tau)$ [$\hat{H}_{\rm eff}(\tau)|\phi_n(\tau)\rangle = \varepsilon_n(\tau)|\phi_n(\tau)\rangle$] and perform the integration over α to obtain Eq. (5). To obtain (6) it suffices to "bracket" Eq. (11) with the same eigenstate and use the Hellmann-Feynman theorem

$$\langle\phi_n(\tau)|\partial_\tau\hat{H}_{\rm eff}(\tau)|\phi_n(\tau)\rangle = \partial_\tau\varepsilon_n(\tau).$$

Finally, to obtain (7), we substitute in Eq. (5) the generalized Hellmann-Feynman theorem

$$\langle\phi_n(\tau)|\partial_\tau\hat{H}_{\rm eff}(\tau)|\phi_m(\tau)\rangle = (\varepsilon_m(\tau)-\varepsilon_n(\tau))\,\langle\phi_n(\tau)|\partial_\tau|\phi_m(\tau)\rangle.$$

DENSITY OF STATES OF $\hat{H}_{\rm ave}$

In order to compute the density of states of $\hat{H}_{\rm ave}$, we take advantage of the symmetries of the model [Eq. (8) in the main text] and restrict ourselves to a single sector with total momentum $k=0$, magnetization $m_z=1/3$, and parity $p=+1$. For the four system sizes considered in our study $L=15$, 18, 21, and 24, the number of states in that sector are $D=111$, 561, 2829, and 15581, respectively.

In Fig. 4, we show the density of states of $\hat{H}_{\rm ave}$ for the three largest systems considered. The lines are fits that make apparent that the density of states are well described by Gaussians. In the inset, we plot the total width of the spectrum, $W=\epsilon_{\rm ave}^{\rm max}-\epsilon_{\rm ave}^{\rm min}$, and the width of the fitted Gaussian $\sqrt{\sigma^2}$ vs the number of spins L. Their scaling is consistent with the expected linear dependence. Note that W and σ were used to define the periods $T_1=2\pi\hbar/W$, $T_2=\pi\hbar/\sigma$, and $T_3=2\pi\hbar/\sigma$ in the main text, which are all expected to collapse to zero in the thermodynamic limit as they scale $\propto L^{-1}$.

PHASE REPULSION IN CIRCULAR ENSEMBLES

In what follows we are interested in understanding the functional form of the probability distribution $P(r)$, where

$$r \equiv \frac{\min(\delta_n,\delta_{n+1})}{\max(\delta_n,\delta_{n+1})} \in (0,1), \tag{12}$$

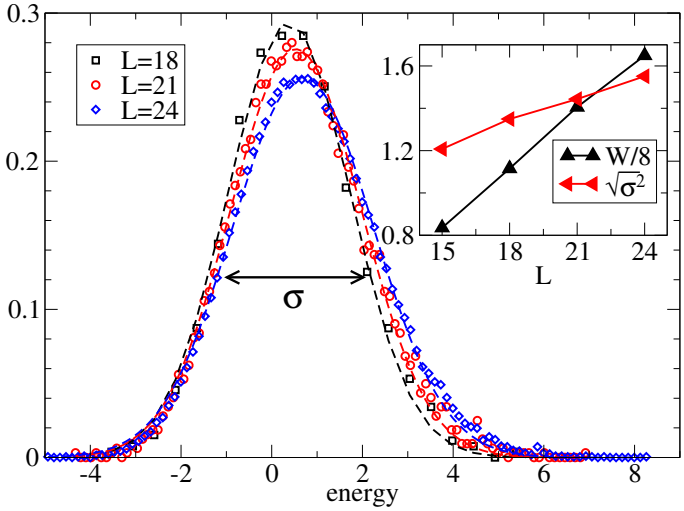

FIG. 4. (Color on-line) Density of states of $\hat{H}_{\rm ave}$, and the best Gaussian fit (dotted lines), for different system sizes L. (Inset) Total width of the spectrum, $W = \epsilon_{\rm ave}^{\rm max} - \epsilon_{\rm ave}^{\rm min}$, and width of the fitted Gaussian, $\sqrt{\sigma^2}$, vs L. The scaling seen for both quantities is consistent with L^1.

in different ensembles. In Gaussian ensembles (GEs), $\delta_n \equiv \epsilon_{n+1} - \epsilon_n$ is the n-th energy gap while in Circular ensembles (CEs) $\delta_n \equiv \theta_{n+1} - \theta_n$ is the n-th phase gap. $P(r)$ has been shown to be a sensitive and practical probe [34, 35] (especially because no-unfolding procedure is necessary) of the integrability-to-chaos transition [36]. For the GEs, the distribution $P(r)$ has been recently calculated [35] starting from the joint distribution of the eigenvalues of a 3×3 random matrix. We now repeat the calculation for a 3×3 random matrix in the CEs.

The joint distribution for the phases in the Circular Orthogonal Ensemble (COE), the Circular Unitary Ensemble (CUE), and Circular Symplectic Ensemble (CSE) are [26–29]:

$$\rho(\theta_1, \cdots, \theta_n) = \frac{1}{Z_{n,\beta}} \prod_{1 \le k < j \le n} |e^{i\theta_k} - e^{i\theta_j}|^\beta, \quad \text{where} \quad Z_{n,\beta} = (2\pi)^n \frac{\Gamma\left(\frac{\beta n}{2} + 1\right)}{\left[\Gamma\left(\frac{\beta}{2} + 1\right)\right]^n},$$

and $\beta = 1, 2, 4$ for COE, CUE and CSE, respectively. For a 3×3 matrix the expression simplifies to:

$$\rho(\theta_1, \theta_2, \theta_3) = \frac{2^{3\beta}}{Z_{3,\beta}} \left|\sin\left(\frac{\theta_1 - \theta_2}{2}\right)\right|^\beta \left|\sin\left(\frac{\theta_1 - \theta_3}{2}\right)\right|^\beta \left|\sin\left(\frac{\theta_2 - \theta_3}{2}\right)\right|^\beta$$

where $\theta_i \in (0, 2\pi)$ [this follows from the normalization $\iiint_0^{2\pi} d\theta_1 d\theta_2 d\theta_3 \rho(\theta_1, \theta_2, \theta_3) = 1$]. We now choose one of the possible six ordering of the angles, $\theta_1 \le \theta_2 \le \theta_3$, define the variable of interest in one of the possible three ways $\delta\left(\tilde{r} - \frac{\theta_2 - \theta_1}{\theta_3 - \theta_2}\right)$, and perform the change of variables $x = \theta_2 - \theta_1, \theta_2, y = \theta_3 - \theta_2$ to obtain:

$$P(\tilde{r}) = \frac{2\pi}{3} \frac{6\, 2^{3\beta}}{Z_{3,\beta}} \int_0^{2\pi} dx \int_0^{2\pi - x} dy \left(\sin\frac{x}{2} \sin\frac{y}{2} \sin\frac{x+y}{2}\right)^\beta \delta\left(\tilde{r} - \frac{x}{y}\right) \tag{13}$$

where the factor of 2π comes from the integration $\int_0^{2\pi} d\theta_2$, the factor of 6 comes from the choice of the ordering, and the factor of 3 comes from the choice of the observable. We also used the identity $\sin\frac{2\pi - x - y}{2} = \sin\frac{x+y}{2}$. The limits of integration in Eq. (13) come from the fact that $0 \le x + y \le 2\pi$ (see Fig. 5). In Eq. (13), $\tilde{r} = \delta_1/\delta_2 \in (0, \infty)$ and is different from r defined in Eq. (12). Luckily, the relation between $P(\tilde{r})$ and $P(r)$ is a simple one, $P(r) = 2P(\tilde{r})\Theta(1 - \tilde{r})$ [35]. The integration in (13) can be performed exactly, we have used *Mathematica*. For example, the distribution for the COE is:

$$P_{\rm COE}(r) = \frac{2}{3}\left(\frac{\sin\left(\frac{2\pi r}{r+1}\right)}{2\pi r^2} + \frac{1}{(r+1)^2} + \frac{\sin\left(\frac{2\pi}{r+1}\right)}{2\pi} - \frac{\cos\left(\frac{2\pi}{r+1}\right)}{r+1} - \frac{\cos\left(\frac{2\pi r}{r+1}\right)}{r(r+1)}\right)$$

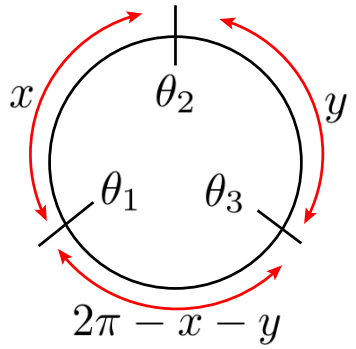

FIG. 5. (Color on-line) The transformation between $\theta_1, \theta_2, \theta_3$ and x, θ_2, z. The limits of integration in Eq. (13) come from the fact that $0 \leq x + y \leq 2\pi$.

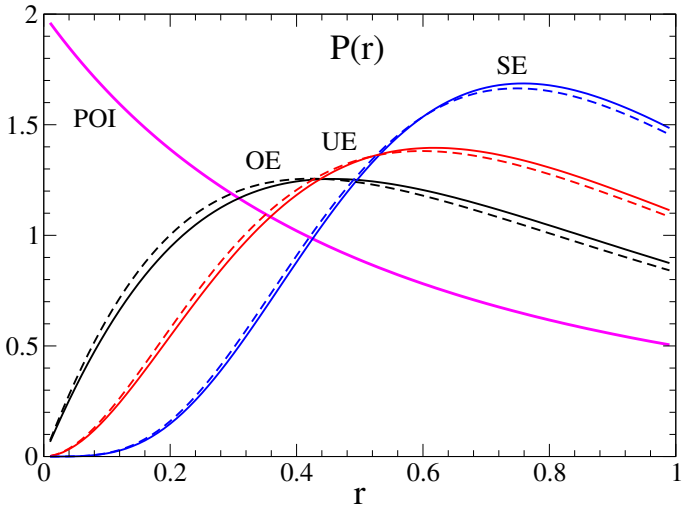

FIG. 6. (Color on-line) The distribution $P(r)$ in the Gaussian and Circular ensembles of random matrix theory and for a sequence of Poisson distributed random numbers. The label POI refers to Poisson while the labels OE, UE, SE refer to Orthogonal, Unitary, and Symplectic Ensembles, respectively. Continues lines depict results for the Gaussian ensembles while dotted lines depict results for the Circular ensembles.

For the sake of brevity the expressions for the CUE and CSE are not reported. In Fig. (6), we plot the distributions $P_{\rm COE}(r)$, $P_{\rm CUE}(r)$, $P_{\rm CSE}(r)$ and compare them with the corresponding distribution for the GEs [$P_{\rm GOE}(r)$, $P_{\rm GUE}(r)$, $P_{\rm GSE}(r)$] and the distribution for a Poisson sequence of random numbers, $P_{\rm POI}(r)$. The distributions for the CE and the corresponding GE are very close for 3×3 matrices and are expected to coincide in the thermodynamic limit. In fact, the phases in the Circular Ensembles (CEs) are expected to have the same local fluctuation properties as the eigenvalues of the corresponding Gaussian Ensembles (GEs) [29]. In Table I, we report the average value of r for all the distributions considered.

Finally, we report numerical results for the model studied in the main text [see Eq. (8)] when $L = 24$. In Fig. 7, we compare the full distribution $P(r)$ for both the exact phases (obtained from the exact diagonalization of $\hat{U}_{\rm cycle}$) and the phases one obtains if $\hat{H}_F = \hat{H}_{\rm ave}$, $\theta_n^{\rm ave} = T\epsilon_n^{\rm ave}/\hbar$, at the periods T_1, T_2, T_3 (see Fig. 1 in the main text) with the GOE, COE and POI predictions. These plots show that at T_1 and T_3 the numerical results for the exact phases

$\langle r \rangle$	Orthogonal	Unitary	Symplectic
Gaussian Ensembles	0.535898	0.602658	0.676168
Circular Ensembles	0.526922	0.596543	0.671921

TABLE I. (Color on-line) Average value of r [see Eq. (12)] in the Gaussian and Circular ensembles of Random Matrix. For comparison the average value of r for a sequence of Poisson distributed random numbers is $\langle r \rangle_{\rm POI} = 0.386294$.

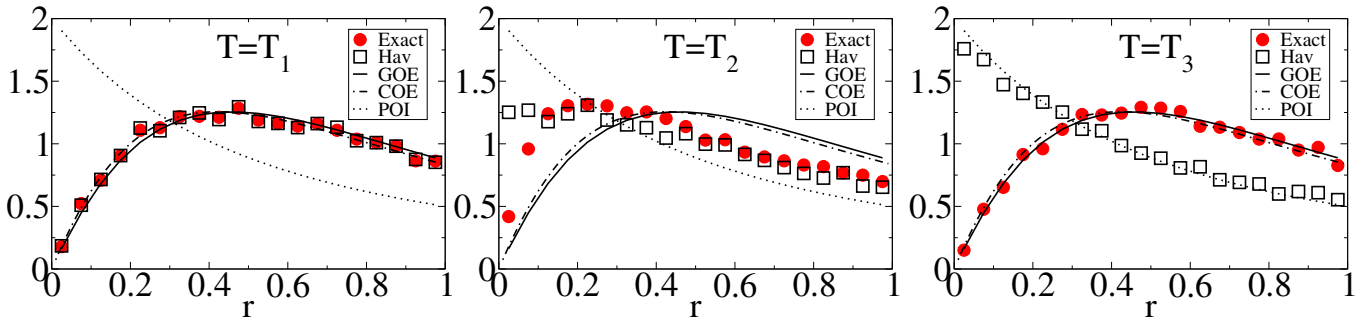

FIG. 7. (Color on-line) Distribution $P(r)$ at the different periods $T = T_1$, T_2, T_3 defined in Fig. 1 in the main text. We compare the exact phases (obtained from the exact diagonalization of $\hat{U}_{\rm cycle}$) (indicated by red circles) and the phases one obtains if $\hat{H}_F = \hat{H}_{\rm ave}$, $\theta_n = T\epsilon_n^{\rm ave}/\hbar$ (indicated by squares), with the GOE, COE and POI predictions (lines).

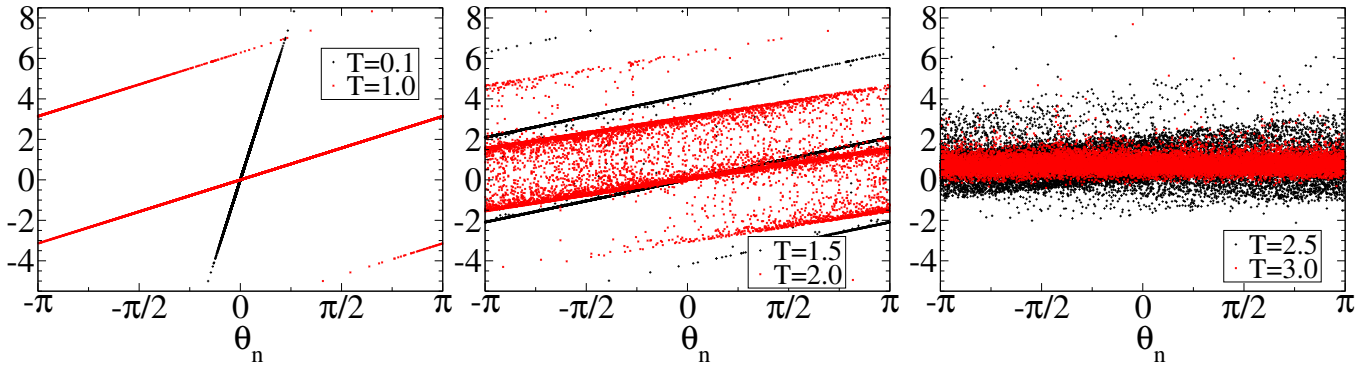

FIG. 8. (Color on-line) Expectation values $\langle\phi_n|\hat{H}_{\rm ave}|\phi_n\rangle$ vs θ_n for $L = 24$ and different driving periods T.

are virtually indistinguishable from the predictions for 3×3 matrices in the GOE and the COE. On the other hand the phases $\theta_n^{\rm ave}$ are clearly described by Poisson statistics at T_3.

EXPECTATION VALUES OF $\hat{H}_{\rm ave}$ IN THE FLOQUET EIGENSTATES

We now investigate the dependence of the expectation values $\langle\phi_n|\hat{H}_{\rm ave}|\phi_n\rangle$ on the phases θ_n for $L = 24$ and different driving periods T. $|\phi_n\rangle$ and θ_n are the exact eigenstates and eigenvalues of the evolution operator over a cycle, i.e. $\hat{U}_{\rm cycle} = \sum_n |\phi_n\rangle e^{-i\theta_n}\langle\phi_n|$. For short periods, the Floquet eigenstates, $|\phi_n\rangle$, are closely related to the eigenstates of $\hat{H}_{\rm ave}$ and the simple relation $\theta_n = \frac{T}{\hbar}\langle\phi_n|\hat{H}_{\rm ave}|\phi_n\rangle$ holds. We note that the phases θ_n might or might not span the entire "Floquet Brillouin zone", i.e. $(-\pi, \pi)$, depending on the value of the period T (see left panel in Fig. 8). For large periods $\hat{U}_{\rm cycle}$ shares the properties of the matrix of the Circular Ensemble and the Floquet eigenstates are essentially random vectors. In this regime the expectation values $\langle\phi_n|\hat{H}_{\rm ave}|\phi_n\rangle$ approach an n-independent value and they are not related to the values of the Floquet phases θ_n (see right panel in Fig. 8). For even larger periods the eigenstate to eigenstate variation of $\langle\phi_n|\hat{H}_{\rm ave}|\phi_n\rangle$ decreases (see inset in Fig. 3 in the main text). For intermediate periods, there is a crossover region in which the relation between θ_n and $\langle\phi_n|\hat{H}_{\rm ave}|\phi_n\rangle$ is progressively lost by increasing the period T (see central panel in Fig. 8).

[1] G. Casati, B.V. Chirikov, F.M. Izrailev and J. Ford, Lecture Notes in Physics **93**, 334-352 (Springer, N.Y. 1979).

[2] B.V. Chirikov and F.M. Izrailev and D.L. Shepelyansky, Soviet Scientific Reviews. Section C **2**, 209 (1981).

[3] S. Fishman and D. R. Grempel and R. E. Prange, Phys. Rev. Lett. **49**, 509-512 (1982).

[4] P.L. Kapitza, Soviet Phys. JETP **21**, 588 (1951).

[5] H.W. Broer and I. Hoveijn and M. van Noort and C. Simo' and G. Vegter, Journal of Dynamics and Differential Equations **16**, 897-947 (2004).

[6] S. Iwai, M. Ono, A. Maeda, H. Matsuzaki, H. Kishida, H. Okamoto, and Y. Tokura, Phys. Rev. Lett. **91**, 057401 (2003).

[7] Z. Ovadyahu, Phys. Rev. Lett. **108**, 156602 (2012).

[8] S. Kaiser, D. Nicoletti, C. R. Hunt, W. Hu, I. Gierz, H. Y. Liu, M. Le Tacon, T. Loew, D. Haug, B. Keimer, A. Cavalleri, arXiv:1205.4661v5.

[9] T. Oka and H. Aoki, Phys. Rev. B **79**, 081406(R) (2009).

[10] T. Kitagawa, T. Oka, A. Brataas, L. Fu, E. Demler, Phys. Rev. B **84**, 235108 (2011).

[11] T. Iadecola, D. Campbell, C. Chamon, C.-Y. Hou, R. Jackiw, S.-Y. Pi, S. V. Kusminskiy, Phys. Rev. Lett. **110**, 176603 (2013).

[12] N. H. Lindner, G. Refael, V. Galitski, Nature Physics **7**, 490-495 (2011).

[13] Y. H. Wang, H. Steinberg, P. Jarillo-Herrero, N. Gedik, Science **25**, 453-457 (2013).

[14] L. D'Alessio and A. Polkovnikov, Annals of Physics **333**, 19-33 (2013).

[15] S. De Sarkar, R. Sensarma, K. Sengupta, arXiv:1308.4689.

[16] C. A. Parra-Murillo, J. Madroero, and S. Wimberger, Phys. Rev. A **88**, 032119 (2013).

[17] C. A. Parra-Murillo, S. Wimberger, Acta Phys. Pol. A **124**, 1091 (2013).

[18] Kai Ji and B. V. Fine, Phys. Rev. Lett. **107** 050401 (2011).

[19] A. Eckardt, C. Weiss and M. Holthaus, Phys. Rev. Lett. **95**, 260404 (2005).

[20] S. Koghee, Lih-King Lim, M. O. Goerbig, C. M. Smith, Phys. Rev. A **85**, 023637 (2012).

[21] M. Matti Maricq, Phys. Rev. B **25**, 6622 (1982).

[22] M. Matti Maricq, Phys. Rev. B **37**, 7215-7229 (1988)

[23] W. Magnus, Commun. Pure Appl. Math. **VII**, 649 (1954).

[24] S. Blanes, F.Casas. J. A. Oteo and J.Ros, Physics Report **470**, 151-238 (2009).

[25] See Supplementary Material

[26] F. J. Dyson, J. Math Phys, **3**, 140 (1962); idem **3**, 157 (1962); **3**, 166 (1962),

[27] M. L. Mehta, *Random Matrices*, Volume 142, Third Edition, Elsevier (2004),

[28] F. Haake *Quantum Signatures of Chaos*, (Springer, Berlin, 3rd ed. 2010).

[29] T. Guhr, A. Muller-Groeling, H. A. Weidenmuller, Physics Reports **299**, 189-425 (1998).

[30] D. Li, Y. Dong, R. G. Ramos, J. D. Murray, K. MacLean, A. E. Dementyev, and S. E. Barrett, Phys. Rev. B **77**, 214306 (2008).

[31] M. Srednicki, Phys. Rev. E **50**, 888 (1994); J. M. Deutsch, Phys. Rev. A **43**, 2046 (1991); M. Srednicki, J. Phys. A **32**, 1163 (1999).

[32] M. Rigol, V. Dunjko, M. Olshanii, Nature **452**, 854 (2009); E. Khatami, G. Pupillo, M. Srednicki, M. Rigol, Phys. Rev. Lett. **111**, 050403 (2013).

[33] L. F. Santos and M. Rigol, Phys. Rev. E **81**, 036206 (2010); ibib. **82**, 031130 (2010).

[34] V. Oganesyan, D. Huse, Phys. Rev. B **75**, 155111 (2007). G. Biroli, A. C. Ribeiro Teixeira and M. Tarzia, arXiv:1211.7334v2.

[35] Y. Y. Atas, E. Bogomolny, O. Giraud, and G. Roux, Phys. Rev. Lett. **110**, 084101 (2013).

[36] L. E. Reichl, *The transition to Chaos: Conservative Classical Sysstems and Quantum Manifestations* (Springer, New York, 2004).

[37] V. Galitski, Phys. Rev. A **84**, 012118 (2011).

[38] V. M. Galitsky, S. P. Goreslavskii and V. F. Elesin, Zh. Eksp. Teor. Fiz. **57**, 207-217 (1969).

[39] D. W. Hone, R. Ketzmerick, and W. Kohn, Phys. Rev. E **79**, 051129 (2009).

[40] M. Langemeyer and M. Holthaus, Phys. Rev. E **89**, 012101 (2014).